Fullerenes, Nanotubes and Carbon Nanostructures

ISSN: 1536-383X (Print) 1536-4046 (Online) Journal homepage: http://www.tandfonline.com/loi/lfnn20

Obtaining of hydroxylated fullerenes Y@$C_{82}O_X$(OH)Y, Y2@C82OX(OH)Y, Y2C2@C82OX(OH)Y and electrophysical characteristic of composite film based thereon

Grigory N. Churilov, Alexander I. Dudnik, Nikolay A. Drokin, Natalia G. Vnukova, Evgeniy V. Tomashevich & Vitaliy S. Bondarev

To cite this article: Grigory N. Churilov, Alexander I. Dudnik, Nikolay A. Drokin, Natalia G. Vnukova, Evgeniy V. Tomashevich & Vitaliy S. Bondarev (2018): Obtaining of hydroxylated fullerenes Y@$C_{82}O_X$(OH)Y, Y2@C82OX(OH)Y, Y2C2@C82OX(OH)Y and electrophysical characteristic of composite film based thereon, Fullerenes, Nanotubes and Carbon Nanostructures

To link to this article: https://doi.org/10.1080/1536383X.2018.1501559

Published online: 21 Nov 2018.

FULLERENES, NANOTUBES AND CARBON NANOSTRUCTURES
https://doi.org/10.1080/1536383X.2018.1501559

Obtaining of hydroxylated fullerenes $Y@C_{82}O_X(OH)Y$, Y2@C82OX(OH)Y, Y2C2@C82OX(OH)Y and electrophysical characteristic of composite film based thereon

Grigory N. Churilov[a,b], Alexander I. Dudnik[a,b], Nikolay A. Drokin[a], Natalia G. Vnukova[a,b], Evgeniy V. Tomashevich[c], and Vitaliy S. Bondarev[a,b]

[a]Kirensky Institute of Physics, Federal Research Center KSC SB RAS, Krasnoyarsk, Russia; [b]Siberian Federal University, Krasnoyarsk, Russia; [c]Institute of Chemistry and Chemical Technology Federal Research Center KSC, SB RAS, Krasnoyarsk, Russia

ABSTRACT

The article presents, for the first time, the results of the research on composite film obtained from hydroxylated endohedral metallofullerenes (EMF) $Y@C_{82}$, $Y_2@C_{82}$, with $Y_2C_2@C_{82}$ and highest fullerenes as dopant. The composite film has been established to have electric conductivity and to be a ferroelectric with the value of residual polarization of ~0.75 $\mu C/cm^2$. The impedance spectroscopy of this sample allowed us to determine dispersion of dielectric permittivity and conductivity in the range of frequencies of 0.5 Hz–100 MHz. It is stated that the value of the high-frequency dielectric permittivity of films is $\varepsilon'_\infty = 2.8$. However, with reduction in the electric field frequency, real and imaginary parts of ε increase to values $\sim 10^4$–10^5. Such increase in dielectric permittivity is connected with increase in polarizing caused by accumulation of mobile electric charges (electrons of ions, protons) on boundaries of the structural defects of a film, which are divided by thin dielectric interlayers. The film is solid electrolyte with the ionic conductivity of $\sim 5 \times 10^{-7}$ S/cm.

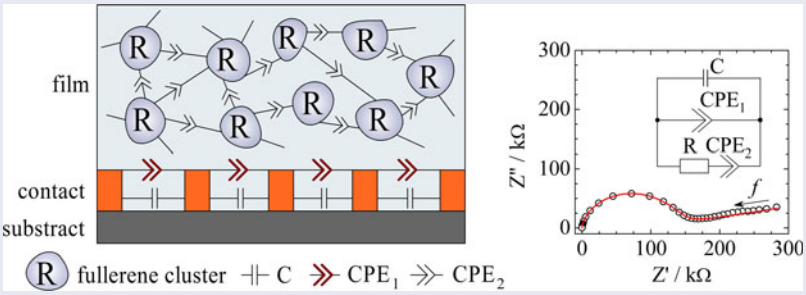

ARTICLE HISTORY
Received 20 June 2018
Accepted 14 July 2018

KEYWORDS
Endohedral metallofullerene; impedance spectroscopy; polarization

1. Introduction

Common fullerenes, with molecules of empty framework, are applied in many fields of science and technology [1–8]. Endohedral metalfullerenes, substances molecules of which consist of the carbon atoms located on the quasispherical closed surface, containing one or several metal atoms, are of special interest. Carbon atoms framework has the generalized π-system of electrons which includes valence electrons of guest atom. Substances, molecules of which are arranged in such unique way, are interesting from the fundamental and applied point of view [9–14]. The presence of the magnetic moment [15] in EMF with rare-earth elements has defined the line of EMF research, i.e. using it as the contrast agent for a magnetic resonance tomography [16–18]. For this EMF is functionalized, i.e. radicals of different degree of complexity are attached to a molecule framework in order to prevent them from dissolving in water or other high-polarity liquids.

Simple functionalization is hydroxylation, addition of OH groups. For hydroxylation of fullerenes KOH or NaOH are usually used [19]. In the fullerenol, obtained via such method, either alkali ions typically present, or K and Na adjoin the molecule framework. Therefore, to obtain a pure fullerenol, we have decided to use a method in which fullerenes are processed by HNO_3 acid. Following the drying of fullerenol solutions, the composite, containing solvent molecules, is formed.

Despite the simplicity of the used hydroxylation methods, we have not encountered researches on electric and dielectric properties of hydroxylate EMF in the literature. The main reason for this is the complexity of synthesis and extraction of pure EMF in quantities, sufficient for carrying out such experiments. Moreover, in the process of

CONTACT Grigory N. Churilov Churilov@iph.krasn.ru Kirensky Institute of Physics, Federal Research Center KSC SB RAS, Krasnoyarsk, Russia.
Color versions of one or more of the figures in the article can be found online at www.tandfonline.com/lfnn.

hydroxylation a considerable amount of EMF perishes or remains on the surface of filters and chemical vessels. Therefore, the purpose of our article was to synthesize the hydroxylate EMF and to search for new application of EMF. Chemical and electrophysical properties of hydroxylate EMF depend on quantity and position of OH groups on the molecule framework surface [20]. Besides the possible presence of dipolar moment, hydroxylate EMF are interesting from the point of view of the ionic conductivity, which is present in common hydroxylate fullerenes. As dopant, the extracted hydroxylate fullerene has $Y_2C_2@C_{82}$ and some highest fullerenes.

We have developed a setup for high-yield synthesis of carbon condensate high in EMF [21]. Using this setup and modern methods of EMF extraction, we have received a compound of hydroxylated fullerene $Y@C_{82}$, $Y_2@C_{82}$ in quantities, sufficient for carrying out researches. Structural and electrophysical properties of EMF were investigated by methods of X-ray photoelectron spectroscopy (XPS), impedance spectroscopy and positive up negative down (PUND). Despite the fact that we have obtained the mixture of EMF and highest fullerenes, such research is conducted for the first time.

2. Materials and methods

Fullerene synthesis was carried out using, developed by us, technique of receiving carbon condensate in high-frequency arc discharge [21]. For the spectral analysis, carbon rods with a diameter of 6 mm had a hole filled to a mixture of graphite powders and Y_2O_3. Fullerenes were extracted in Soxhlet extractor with the use of carbon disulfide. The quantity of EMF in the fullerenes mixture amounted to 7wt%. The quantity was determined using the technique developed by us, which included mass and spectral researches, XPS, and the atomic and issue analysis. Further EMF enrichment, using the technique based on use of Lewis acids $TiCl_4$ [22] was carried out. Then the mixture of fullerenes was dried up and dissolved in toluene. Fullerene fission was carried out on the chromatograph of Agilent Technologies 1200 Series (the column Cosmosil Buckyprep M; toluene stream of 5 ml/min). The chromatographic fraction has been certified by method of mass spectrometry (MALDI-TOF Bruker BIFLEX TM III) which has shown that substance consists of two types of EMF $Y@C_{82}$, $Y_2@C_{82}$, with a small amount of $Y_2C_2@C_{82}$ dopant and the highest fullerenes. The addition of OH group to EMF was carried out via the simplified technique [23]: boiling in the concentrated HNO_3 for 4 h, triple washing in the distilled water and filtration.

Then, water solution of hydroxylate EMF was shed in small drops onto the sensor. After applying every portion of solution, we set the solvent to evaporate at a temperature of 20 °C and leave a fullerenol powder on the sensor. In total, 2 ml of the concentrated solution have been shed. Prior to measurements of impedance, the received film and the measuring sensor were dried at a temperature of approximately 40 °C within 3 days for electrical characteristics stabilization. The film did not slough off the sensor even under vibration.

The measuring instrument was manufactured in the form of the flat interdigital metalized construction on a corundum ceramic base, which contains six pairs of pivots 5 mm long, 0.2 mm wide with a gap between pivots of 0.1 mm. The film of 30 μm thickness completely covered the surface of interdigital construction. For correct definition of electrophysical characteristics of a fullerene film, preliminary calibration of the sensor was carried out. This process included determination of correlation of experimentally measured effective capacity of the $C_{\text{eff}}(f)$ sensor with the dielectric permittivity (DP) of a number of model materials (Teflon films $\varepsilon = 2.1$, mica covers $\varepsilon = 7$, and some chemically pure liquid dielectrics). The prepared sensor and a sample were connected to the impedance analyzer (Agilent Technologies E5061B). The frequency dependence of the impedance module $|Z|$ and phase angle φ in the frequency range from 0.5 Hz up to 100 MHz was registered. The value of AC current given to a measurement cell did not exceed 0.25 V. The impedance measurements were carried out at a temperature of 20 °C. Ferroelectric properties were investigated on the Easy Check 300 device.

3. Results

3.1. General characteristics of hydroxylated EMF compound

Results of mass-spectral analyses have shown that the extracted fraction contains EMF with $Y@C_{82}$, $Y_2@C_{82}$, $Y_2C_2@C_{82}$ yttrium, as well as the highest fullerenes (Figure 1).

The XPS method has determined elemental composition of a film. Binding energies of carbon were determined by the C1s line (Figure 2). $E_{CB} = 284.2$ eV (21.5%)—carbon in

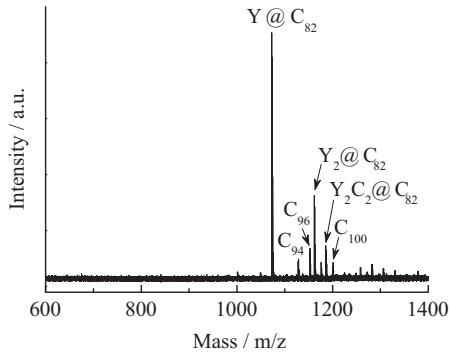

Figure 1. Mass-spectrum (positive ions) detached from chromatographic fraction.

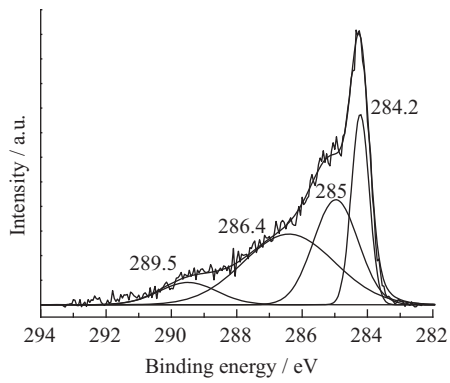

Figure 2. XPS of C1s line of fullerenol film.

hybridization, corresponding to fullerene [24], $E_{CB} = 285$ eV (29.7%)—C–OH, $E_{CB} = 286.4$ eV (40%)—C = O [25, 26]. The highest binding energy is found in carbon in sp^2-hybridization. A small peak at 289.5 eV (8.2%) corresponds to transition of $\pi \rightarrow \pi^*$ in the remained interfaced parts on a molecule framework [26]. Elemental composition of a hydroxylated EMF film estimates to carbon—75.09 at.%, oxygen—24.78 at.%, yttrium—0.13 at.%.

As the received substance is a mixture of several EMFs and the highest fullerenes, it is impossible to tell how many OH group have joined each component. Based on the XPS analysis results of the line C 1s, it is possible to assume that the film consists of hydroxylated EMF and the highest fullerenes with the number of the C = O groups 24 max and C–OH 32 max. The total number of both groups at fullerenol does not exceed 42 [27], and the number of the C = O groups for hydroxylated EMFs does not exceed 12.

3.2. Impedance spectroscopy

Frequency dependence measurements of the impedance module $|Z(f)|$ and a phase $\varphi(f)$ were carried out at a room temperature and then the valid $Z'(f) = |Z(f)| \cdot \cos\varphi(f)$ and imaginary $Z''(f) = |Z(f)| \cdot \sin\varphi(f)$ impedance parts. These values allowed us to define the main electrophysical characteristics of the studied material: effective resistance $R_{eff}(f)$, capacity $C_{eff}(f)$, loss tangent $\mathrm{tg}\delta(f) = Z'(f)/Z''(f)$, real $\varepsilon' = C_{eff}/C_0$ and imaginary $\varepsilon'' = \varepsilon' \cdot \mathrm{tg}\delta$ parts of dielectric permittivity, and specific conductivity $\sigma'(f) = \varepsilon'' \cdot \varepsilon_0 \cdot 2\pi \cdot f$ and $\sigma''(f) = \varepsilon' \ \varepsilon_0 \cdot 2\pi \cdot f$ [28]. The received frequency dependences of DP and specific conductivity are given in Figures 3 and 4.

As shown in Figure 3, at high frequencies of $f \sim 10^8$ Hz, in present film real DP part equal to $\varepsilon' = 2.8$ (*1*) comparable to DP of common fullerenes. However with decrease in frequency of $f < 10^4$ Hz, both real (*1*), and imaginary (*2*) DP parts increase to the value of $\sim 10^5$–10^6. Increase of imaginary part (*2*) happens due to reach-through conductivity of $\sigma'(\omega)$, an increase of real part (*1*) at low frequencies can be explained by process of electric charge accumulation near structural heterogeneity, consisting of conductive dielectric areas of the film. Electric field at the boundaries of such structures is directed opposite to external field and is perceived in the experiment as the seeming increase in DP

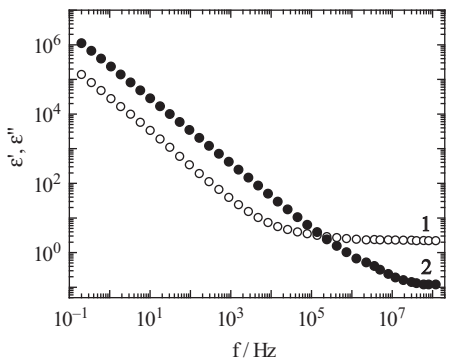

Figure 3. Frequency dependency of real ε' (*1*) and imaginary ε'' (*2*) DP parts.

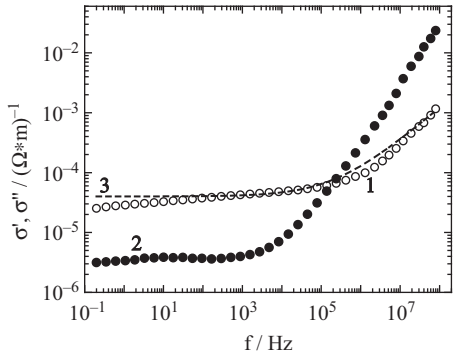

Figure 4. Frequency dependency of real σ' (*1*) and imaginary σ'' (*2*) conductivity parts. Approximation of dependency σ' (f) (*3*).

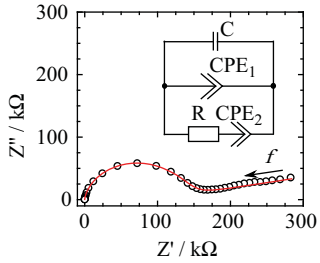

Figure 5. Hodograph of impedance and equivalent diagram.

substance. In the high-frequency range volume charges do not manage to be formed, and DP approaches to the value, common for fullerenes, $\varepsilon_\infty = 2.8$–2.4.

To determine possible electrophysical processes of polarization and transition of charges in the studied sample, it is convenient to present impedance frequency spectrum in the form of the hodograph [1, 14] constructed as dependence of imaginary impedance part Z'' from real part Z' (Figure 5). Certain frequency corresponds to each point of hodograph, and the arrow in the figure specifies the direction in which frequency increases.

As presented, the impedance hodograph consists of two structural elements. One of these elements is a semi-circle arc, formed in the high-frequency range, and another is a direct branch increasing in process of frequency reduction. This type of a hodograph can be compared with the equivalent diagram shown on an inset of Figure 5. The diagram consists of three parallel chains in one of which the common container C_1 is included. In the second chain there is the specific CPE_1 (*constant phase element*), and in lower chain series-connected resistor R_1 and the CPE_2 element are included. The necessity of using CPE elements is caused by presence of a hodograph low-frequency branch and shift of the center of a semi-circle below the vertical axis. The complex CPE impedance contains real and imaginary parts and registers in the form of [27]:

$$Z_{CPE} = \frac{1}{A(i\omega)^\eta} = \frac{1}{A\omega^\eta}\left[\cos\left(\eta\frac{\pi}{2}\right) - i\sin\left(\eta\frac{\pi}{2}\right)\right] \qquad (1)$$

where A is a proportionality ratio, i is an imaginary unit and $0 \leq \eta \leq 1$ is fractional exponent, which indirectly characterizes fractal resistive and capacitive structures of the studied substances. Numerical search of electrical rating

values of elements of this equivalent diagram was carried out with use of the special *EIS Spectrum Analyser* program. For the hodograph given in Figure 5, calculation for the CPE_1 element has shown that coefficient of $A = 5.13 \times 10^{-6}$ and $\eta = 0.12$. For values $\eta < 0.5$, CPE_1 element simulates frequency-dependent resistor which along with the C_1 condenser forms a hodograph semi-circle arc in the high-frequency range.

At low frequencies the slanting branch of a hodograph is well simulated by the static resistance of $R_1 = 96.5$ kΩ and the capacitive element CPE_2 with coefficient $A_2 = 6.74 \times 10^{-11}$ and $\eta = 0.8$. Such exponent generally demonstrates the presence of distributed capacity in the studied film, which can appear due to accumulation of electric charges on boundaries of heterogeneous film structures. It also is the reason for increased real and imaginary DP parts in the high-frequency range.

As shown in Figure 4, with growth of frequency f to 10^4 Hz both real and imaginary conductivity parts do not significantly depend on frequency in the beginning. However with further increase in frequency both conductivity parts increase rapidly. Imaginary conductivity part increases in logarithmical coordinates almost linearly as $1/(\omega C)$, where C is the high-frequency capacitance of the sample. The increase of real conductivity part can be approximated by the known dependence $\sigma'(\omega) = 4 \times 10^{-5} + 3.2 \times 10^{-8} \times \omega^{0.56}$ with fractional exponent for circular frequency [29]. Usually frequency dependences of this kind arise at implementation of the charge motion hopping mechanism in electric field.

Based on the theory, the imaginary conductivity σ'' in direct proportion depends on frequency. But due to accumulation of charges on structural defects of the film (which also causes increase of ε') the dependence of σ'' on frequency becomes horizontal at low frequencies. Frequency, at which this change happens, is considered the beginning of low-frequency range, where charge carriers can move in between electrodes. On the impedance hodograph given point corresponds to the left border of a linear part, and the peak proton conductivity is determined using this point [30]. Specific conductivity of the studied film (Figure 4) we estimate in 5×10^{-7} Ω cm.

Thus, based on the results of the impedance research, presented film sample should be considered as spatially heterogeneous conductive structure, which in alternating electric field can be strongly polarized at low frequencies. It should be noted that over time there is some degradation of the film: the value and DP frequency dependence changes in a complicated way, the conductivity of the film decreases.

3.3. Residual polarization

Dielectric-hysteresis loops are usually studied according to Sawyer-Tower circuit. However, in present case application of this circuit is impossible. It is connected with the small resistance of the film—600 kΩ at a frequency of 250 Hz which shunts the accumulated charges on electrodes. We have investigated ferroelectric properties by the PUND method [31].

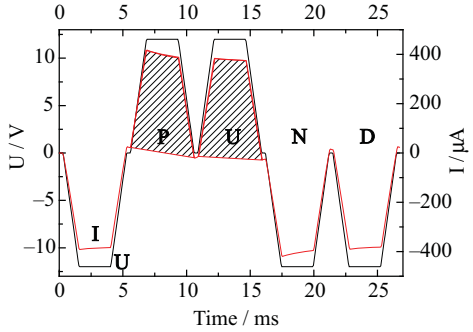

Figure 6. Time dependency of voltage and current applied to the film.

Figure 6 demonstrates the form of voltage enclosed to the resistive-capacitive divider and a form of the current passing through it. The third impulse (U) polarized not all dipoles, but only the part which has returned to a former state after cancelation of the second impulse (P) that corresponds to the presence of residual polarization in the sample. Smooth decrease of current at the constant level of voltage for the 3rd impulse suggests slow rotation of dipoles. The small difference in amplitudes values between 3 and 2 current impulse implies small residual polarization.

Calculating the difference of the areas under current peaks for impulses P and U, we receive value of residual polarization of the $2P_r$ equal to 0.136 μC. Taking into account the area and thickness of the film, the value of $P_r \approx 0.75$ μC/cm^2. The size dimensions of the film on the planar interdigital structure have been counted in an equivalent parallelepiped. Equivalent resistance of the film was estimated as parallel combination of a film part resistance over contacts and part of the film between contacts of the comb.

So far, on the basis of the conducted research, it is early to speak about applying the received fullerenol in pure form as, for example, ferroelectric for condensers as tgδ at low frequencies has quite high value (∼6). However, it is quite possible to use the fullerenol as the substance able to absorb electromagnetic waves in the wide range of frequencies. It can also be used as a dopant to increase ionic conductivity in solid electrolytes, as it is done for Nafiona® by injecting fullerenes and fullerenol [5–7]. If we compare proton conductivity of the substance received by us to conductivity of a $C_{60}OH_{12}$ fullerenol [32], the proton conductivity of the latter is equal to 7×10^{-6} S/cm, a $C_{60}OH_{24}$ fullerenol [33] has conductivity of 10^{-7}–10^{-8} S/cm, and proton conductivity of a hydrolyzed polycyclosulfated fullerene [30] is 10^{-3} S/cm. It is difficult to speak of other advantages as the research has just begun.

4. Conclusion

As a result, it can be concluded that the products received from composites on the basis of hydroxylated EMFs with Y have proton conductivity and ferroelectric properties. Studies have shown that impedance characteristics of a product, in this case film, possesses ε' reaching the value of 10^4 and $\varepsilon'' \sim 10^5$, at frequencies near 10 Hz, as well as small resistance $\sim 10^6$ Ω. Measurements have shown that the film

on the basis of EMF with Y is a ferroelectric material with the value of residual polarization of $P_r \approx 0.75$ $\mu C/cm^2$. Values of imaginary and real parts of dielectric permittivity are connected with the polarization process of charge carriers on boundaries of internal nonhomogeneous regions, as well as with a small active resistance.

Acknowledgments

We thank A.A. Popov and his team (The Leibniz Institute for Solid State and Materials Research, Dresden, Germany) for research conducted via mass-spectrometer MALDI-TOF Bruker BIFLEX TM III.

References

[1] Gunnarsson, O. Superconductivity in Fullerides. *Rev. Mod. Phys*. **1997**, *69*, 575–606.
[2] Tutt, L. W.; Kost, A. Optical Limiting Performance of C_{60} and C_{70} Solutions. *Nature* **1992**, *356*, 225–226.
[3] Tada, T.; Kanayama, T. Nanolithography Using Fullerene Films as an Electron Beam Resist. *Jpn. J. Appl. Phys*. **1996**, *35*, L63–L65.
[4] Aleshin, A. N.; Biryulin, Y. F.; Mironkov, N. B.; Sharonova, L. V.; Fadeeva, E. N.; Zgonnik, V. N. Optical and Electrical Properties of Star-like Fullerene-Containing Polymers. *Fuller. Sci. Technol*. **1998**, *6*, 545–561.
[5] Tasaki, K.; DeSousa, R.; Wang, H. B.; Gasa, J.; Venkatesan, A.; Pugazhendhi, P.; Loutfy, R. O. Fullerene Composite Proton Conducting Membranes for Polymer Electrolyte Fuel Cells Operating under Low Humidity Conditions. *J. Membr. Sci*. **2006**, *281*, 570–580.
[6] Wang, H.; DeSousa, R.; Gasa, J.; Tasaki, K.; Stucky, G.; Jousselme, B.; Wudl, F. Fabrication of New Fullerene Composite Membranes and Their Application in Proton Exchange Membrane Fuel Cells. *J. Membr. Sci*. **2007**, *289*, 277.
[7] Jung, J.-H.; Vadahanambi, S.; Oh, I.-K. Electro-Active Nano-Composite Actuator Based on Fullerene-Reinforced Nafion. *Compos. Sci. Technol*. **2010**, *70*, 584–592.
[8] Woo, Y.; Kim, B.-S.; Lee, J.-W.; Park, J.; Cha, M.; Takeya, S.; Im, J.; Lee, Y.; Jeon, T.-I.; Bae H.; et al. Enhanced Hydrogen: Storage Capacity and Structural Stability of an Organic Clathrate Structure with Fullerene (C_{60}) Guests and Lithium Doping. *Chem. Mater*. **2018**, *30*, 3028–3039.
[9] Kobayashi, S.; Mori, S.; Iida, S.; Ando, H.; Takenobu, T.; Taguchi, Y.; Fujiwara, A.; Taninaka, A.; Shinohara, H.; Iwasa, Y. Conductivity and Field Effect Transistor of $La_2@C_{80}$ Metallofullerene. *J. Am. Chem. Soc*. **2003**, *125*, 8116–8117.
[10] Ross, R. B.; Cardona, C. M.; Guldi, D. M.; Sankaranarayanan, S. G.; Reese, M. O.; Kopidakis, N.; Peet, J.; Walker, B.; Bazan, G. C.; Van Keuren, E.; et al. Endohedral Fullerenes for Organic Photovoltaic Devices. *Nat. Mater*. **2009**, *8*, 208–212.
[11] Harneit, W. Fullerene-Based Electron-Spin Quantum Computer. *Phys. Rev. A* **2002**, 65, 032322.
[12] Larsson, J. A.; Greer, J. C.; Harneit, W.; Weidinger, A. Phosphorous Trapped within Buckminsterfullerene. *J. Chem. Phys*. **2002**, *116*, 7849–7854.
[13] Wharton, T.; Kini, V.; Mortis, R. A.; Wilson, L. J. New Non-Ionic, Highly Water-Soluble Derivatives of C-60 Designed for Biological Compatibility. *Tetrahedron Lett*. **2001**, *42*, 5159–5162.
[14] Yang, H.; Lu, C.; Liu, Z.; Jin, H.; Che, Y.; Olmstead, M. M.; Balch, A. L. Detection of a Family of Gadolinium-Containing Endohedral Fullerenes and the Isolation and Crystallographic Characterization of One Member as a Metal-Carbide Encapsulated inside a Large Fullerene Cage. *J. Am. Chem. Soc*. **2008**, *130*, 17296–17300.
[15] Li, J.; Wang, T.; Feng, Y.; Zhang, Y.; Zhen, M.; Shu, C.; Jiang L.; Wang Y.; Wang C. A Water-Soluble Gadolinium Metallofullerenol: Facile Preparation. *Magn. Prop. Magn. Res. Imag. Appl. Dalton Trans*. **2016**, *45*, 8696–8699.
[16] Takaya, Y.; Tachika, H.; Hayashi, T.; Kokubo, K.; Suzuki, K. Performance of Water-Soluble Fullerenol as Novel Functional Molecular Abrasive Grain for Polishing Nanosurfaces. *CIRP Ann. Manuf. Technol*. **2009**, *58*, 495–498.
[17] Rincón, M. E.; Guirado-López, R. A.; Rodríguez-Zavala, J. G.; Arenas-Arrocena, M. C. Molecular Films Based on Polythiophene and Fullerol: Theoretical and Experimental Studies. *Sol. Energy Mater. Sol. Cells* **2005**, *87*, 33–47.
[18] Li, T.; Dorn, H. C. Biomedical Application of Metal-Encapsulated Fullerene Nanoparticles. *Small* **2017**, *13*, 1603152.
[19] Zhang, J.-M.; Yang, W.; He, P.; Zhu, S.-Z. Efficient and Convenient Preparation of Water-Soluble Fullerenol. *Chin. J. Chem*. **2010**, *22*, 1008–1011.
[20] Tang, J.; Xing, G. M.; Zhao, F.; Yuan, H.; Zhao, Y. L. Modulation of Structural and Electronic Properties of Fullerene and Metallofullerenes by Surface Chemical Modifications. *J. Nanosci. Nanotechnol*. **2007**, *7*, 1085–1101.
[21] Churilov, G.; Popov, A.; Vnukova, N.; Dudnik, A.; Samoylova, N.; Glushenko, G. Controlled Synthesis of Fullerenes and Endohedral Metallofullerenes in High Frequency Arc Discharge. *Fuller. Nanotubes Carbon Nanostruct*. **2016**, *24*, 675–678.
[22] Akiyama, K.; Hamano, T.; Nakanishi, Y.; Takeuchi, E.; Noda, S.; Wang, Z.; Kubuki, S.; Shinohara, H. Non-HPLC Rapid Separation of Metallofullerenes and Empty Cages with $TiCl_4$ Lewis Acid. *J. Am. Chem. Soc*. **2012**, *134*, 9762–9767.
[23] Chiang, L. Y.; Upasani, R. B.; Swirczewski, J. W.; Soled, S. Evidence of Hemiketals Incorporated in the Structure of Fullerols Derived from Aqueous Acid Chemistry. *J. Am. Chem. Soc*. **1993**, *115*, 5453–5457.
[24] Tan, M.; Zhu, J.; Han, J.; Niu, L.; Lu, J.; Chen, W. Relative Fraction of sp^3 Bonding in Boron Incorporated Amorphous Carbon Films Determined by X-Ray Photoelectron Spectroscopy. *Mater. Res. Bull*. **2008**, *43*, 1670–1678.
[25] Xing, G. M.; Zhang, J.; Zhao, Y. L.; Tang, J.; Zhang, B.; Gao, X. F.; Yuan, H.; Qu, L.; Cao, W. B.; Chai, Z. F.; et al. Influences of Structural Properties on Stability of Fullerenols. *J Phys Chem B* **2004**, *108*, 11473–11479.
[26] Iezzi, E. B.; Cromer, F.; Stevenson, P.; Dorn, H. C. Synthesis of the First Water-Soluble Trimetallic Nitride Endohedral Metallofullerols. *Synth. Met*. **2002**, *128*, 289–291.
[27] Wang, B.-C.; Wang, H.-W.; Tso, H.-C.; Chen, T.-L.; Chou, Y.-M. Theoretical Studies of C70(OH)n (n = 14, 16, 18 and 20) Fullerols. *J. Mol. Struct.: THEOCHEM* **2002**, *581*, 177–186.
[28] Barsoukov E.; Macdonald J. R. (ed.). *Impedance Spectroscopy Theory, Experiment and Applications*. Hoboken, New Jersey: John Wiley & Sons, Inc., **2005**.
[29] Dyre, J. C.; Schroder, T. B. Universality of AC Conduction in Disordered Solids. *Rev. Mod. Phys*. **2000**, *72*, 873–892.
[30] Hinokuma, K.; Ata, M. Proton Conduction in Polyhydroxy Hydrogensulfated Fullerenes. *J. Electrochem. Soc*. **2003**, *150*, A112–A116.
[31] Mickaël L. (ed.). *Ferroelectrics: Physical Effects*. Rejika: InTech, **2011**, 77–100.
[32] Hinokuma, K.; Ata, M. Fullerene Proton Conductors. *Chem. Phys. Lett*. **2001**, *341*, 442–446.
[33] Mitsari, E.; Romanini, M.; Barrio, M.; Tamarit, J. L.; Macovez, R. Protonic Surface Conductivity and Proton Space-Charge Relaxation in Hydrated Fullerol. *J. Phys. Chem. C* **2017**, *121*, 4873–4881.